Investigating Fracture Toughness Behavior of CNT and GNP Reinforced Vinyl-ester Resin by Altering Surface Characteristics of the Nanoparticles

C.M. Gapstur*, H. Mahfuz** and A.C. Terentis***

Florida Atlantic University, Boca Raton, FL, USA
Department of Ocean and Mechanical Engineering; *cgapstur@fau.edu; **hmahfuz@fau.edu
Department of Chemistry and Biochemistry; ***terentis@fau.edu

ABSTRACT

In this paper, we compared the fracture toughness (K_{IC}) and strain energy release rate (G_{IC}) of three hybrid inclusion nanocomposite systems. The systems differed by the surface treatment of the included carbon nanotubes (CNT) and graphene nanoplatelets (GNP). Carboxyl (COOH) functionalized CNT (f>CNT) and GNP (f>GNP) and non-functionalized CNT (nf>CNT) and GNP (nf>GNP) were included in vinyl-ester (VE). We employed the surfactant, Triton X-100 (TX100), to surface modify the nanoparticles. Several fabrication and testing iterations revealed an optimized concentration of 0.25wt%-GNP and 0.5wt%-CNT, which produced the highest fracture toughness values. We made samples for fracture toughness tests using the traditional composite synthesis procedures. The three systems we compared were: f>GNP-f>CNT/VE (1); f>GNP-f>CNT-TX100/VE (2); nf>GNP-nf>CNT-TX100/VE (3). Results showed that system 3 exhibited the greatest K_{IC} and G_{IC} increases over neat-VE at 56% and 161%, respectively.

Keywords: fracture toughness, nanocomposites, carbon nanotube, graphene nanoplatelet, surfactant

1 INTRODUCTION

Since the discovery of carbon nanotubes (CNT) by Iijima [1], inorganic nanoparticles have been employed in composites to improve the mechanical, electrical and thermal properties. The four main types of nanomaterials utilized in composites are CNT, GNP, nanoclay and nanosilica. Polymer resin based composites with nanoparticle inclusions (nanocomposites) are widely considered the future of engineering materials because of their attractive properties, such as: strength-to-weight ratio, resistance to corrosion, durability, radar transparency, non-magnetic quality, design flexibility attribute, low thermal conductivity and dimensional stability.

In advanced engineering materials selection, one of the most important properties is the damage tolerance, also known as fracture toughness, of the material. Fracture toughness measures the ability of the material to resist the growth of a crack and to resist fracture. When compared to other engineering materials, polymer composites are known to have low fracture toughness. Past reasearch on the fracture toughness of polymers has mostly focused on a single-type nanoparticle inclusion strategy. We have chosen to focus on a hybrid (dual-type) nanoparticle inclusion strategy.

Because VE has fewer open sites in its molecular chain, it is less sensitive to humidity and temperature and more resistant to corrosion. Moreover, VE enjoys higher K_{IC} and G_{IC} values, when compared to other epoxy resins [2]. For these reasons, we selected VE as our polymer.

We chose CNT, a one-dimensional (1D) carbon allotrope, and GNP, a two-dimensional (2D) carbon allotrope, as the nanofillers because of their well known strength and thermal features. Because CNT and GNP tend to agglomerate due to their van der Waals Forces and the aspect ratios of CNT, they are difficult to disperse in polymer matrices [3]. Non-uniform and disorderly nanoparticle dispersions yield inferior mechanical and thermal properties of the resulting nanocomposite. To minimize nanoparticle agglomerations in our nanocomposites, we selected TX100 as the nanoparticle surfactant. TX100 has been shown to have the highest nanoparticle dispersive power, when compared to other common surfactants [4]. The two types of CNT and GNP used in this reasearch were COOH functionalized and non-functionalized. Both types were surface treated by TX100.

The three compared optimized hybrid nanocomposites (OHN) systems were the first time both CNT and GNP were successfully included in VE matrix. By altering the surface characteristics of the included CNT and GNP, our goal was to further enhance the fracture toughness of the OHN. We also aimed to retain or augment the nanocomposite mechanical and thermal traits.

2 EXPERIMENTAL

2.1 Materials

Sigma-Aldrich (St. Louis, MO, USA) supplied carboxyl acid functionalized multi-walled carbon nanotubes (MWCNT) and Triton X-100. CheapTubes Inc. (Cambridgeport, VT, USA) provided carboxyl acid functionalized graphene nanoplatelets, non-functionalized multi-walled carbon nanotubes and non-functionalized graphene nanoplatelets. Ashland Composites (Dublin, OH, USA) furnished Derakane 8084 vinyl-ester resin. We obtained other necessary chemicals used for the synthesis of nanocomposites from Sigma-Aldrich, Fisher Scientific

International (Hampton, NH, USA), VWR International (Radnor, PA, USA) and United Initiators (Elyria, OH, USA).

2.2 Surface Treatment

Two of the three systems compared within this paper contained nanoparticles that were surface treated by the surfactant Triton X-100. First, we added the specified mass of CNT and GNP to a beaker. We then included TX100 to the beaker at a ratio of 2:1 (TX100 mass to CNT+GNP mass). Next, we introduced the solvent, acetone, into the mixture at a ratio of 100mL:0.1g (acetone to CNT+GNP mass). To aid in surface absorption of TX100 onto the CNT and GNP surfaces, we initiated mechanical stirring at 500rpm for 30 minutes. The stirred mixture subsequently underwent ultrasonication for 30 minutes at an amplitude of 40%. The ultrasonication process imparted approximately 40kJ of cavitation energy. Lastly, we stored the beaker in a ventilated area for roughly one week to allow the acetone to offgas. The final product consisted of a black, oily layer of TX100 treated nanoparticles on the bottom of the beaker.

2.3 Specimen Fabrication and Preparation

Depending on the system selected for fabrication, we placed the CNT and GNP with appropriate surface characteristics in a beaker. We then added the calculated mass of VE to the beaker to reach a final nanocomposite sample with concentrations of 0.25wt%-GNP and 0.5wt%-CNT. A mechanical stirrer mixed the polymer-nanoparticle admixture at 300rpm for 15 minutes. We sonicated the admixture for 15 minutes at an amplitude of 40%. Next, we placed the admixture under a vacuum in a desicator chamber for 15 minutes. Subsequently, we incorporated hardeners and initiators into the admixture via mechanical stirring. We poured the admixture into silicon molds. Fabricated specimens cured at room temperature in the silicon molds for approximately 24 hours. The specimens later post-cured in a kiln at 120°C for two hours. Each nanocomposite batch yielded two specimens with dimensions of approximately 112mm (L) x 24mm (W) x 12mm (B), as illustrated in Figure 1. The dimensions complied with the geometric criteria stated in the fracture toughness testing standard (ASTM D5045-14) used in this research [5].

Once post-cured, we further prepared the specimens for ASTM D5045-14 testing [5]. We progressively polished the top and bottom surfaces of each specimen with sanding paper of the following grit: 80, 100, 400 and 2000. Using a bandsaw, we machined a sharp notch into the bottom surface of one specimen from each batch. The notch length (a) measured at least half the width of the specimen. We induced a natural crack at the tip of the notch by utilizing a fresh razor blade in a sawing motion. Fabrication and preparation procedures resulted in one un-cracked (indentation) and one cracked specimen per nanocomposite batch.

2.4 Mechanical Characterization

To determine the K_{IC} and G_{IC} of each nanocomposite specimen, we employed the Standard Test Methods for Plain-Strain Fracture Toughness and Strain Energy Release Rate of Plastic Materials (ASTM D5045-14) in single-edge-notch bending (SENB) testing configuration, as shown in Figure 1 [5]. We used a Zwick-Roell testing machine in flexure mode with the Standard designated crosshead rate of 10mm/min and at the Standard proposed testing ambient temperature of 23°C [5].

Using the cracked specimen from each batch, we calculated the fracture toughness, K_Q, according to Equation 1, where K_Q was the conditional K_{IC} [5]. P_Q was the load applied when testing the cracked specimen and cooresponded to a 5% increased compliance [5]. To ensure test validity, P_{max} divided by P_Q was less than or equal to 1.1 [5]. Furthermore, f(x) was the geometric shape factor [5]. According to the Standard, the fracture toughness test of each cracked specimen was acceptable when thickness (B), crack length (a) and ligament (W-a) were greater than the value of Equation 2, where σ_y was the yield stress of the specimen [5].

To calculate the strain energy release rate, G_Q, we utilized the load-displacement curves produced from the fracture toughness test for both the cracked and un-cracked specimens. We computed the areas underneath the load-displacement curves for the cracked and un-cracked specimens and took them as U_Q and U_i, respectively. We then corrected for compliance, loading-pin and support indentation by subtracting U_i from U_Q to get U. From Equation 3, we took GIC as GQ, where ϕ was the energy calibration factor that the Standard provided [5].

$$K_Q = P_Q f(x)/BW^{1/2} \quad (1)$$

$$2.5(K_Q/\sigma_y)^2 \quad (2)$$

$$G_Q = U/(BW\phi) \quad (3)$$

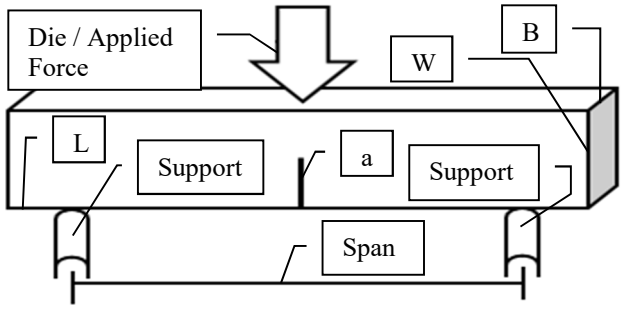

Figure 1: Specimen configuration and test setup for the SENB fracture toughness test.

2.5 Thermal Characterization

We determined thermal properties of the nanocomposite specimens through the use of the following studies: differential scanning calorimetry (DSC); thermogravimetric analysis (TGA); dynamic mechanical analysis (DMA). Using the DSC and DMA results, we calculated the glass

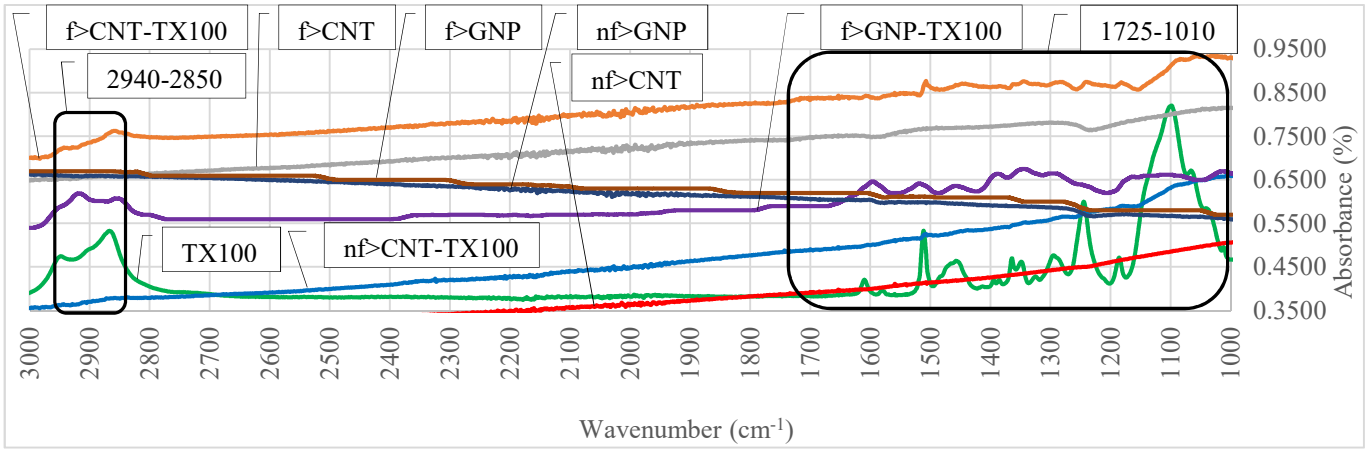

Figure 2: FTIR spectra for nanoparticles used in this study.

transition temperature (T_g) of the nanocomposites according to ASTM E1346-08 [6]. To derive the maximum thermal decomposition temperature (T_p), we used the TGA curves to compute the derivative TGA (DTG) curves. The DTG curves pinpointed the T_p for each nanocomposite specimen.

2.6 Spectroscopic Characterization

To establish the surface characteristics of the nanoparticles used in this investigation, we utilized fourier-transform infrared spectroscopy (FTIR). We also examined the extent of TX100 nanoparticle surface treatment through visual inspection of nanoparticles in solution.

3 RESULTS AND DISCUSSION

3.1 Nanoparticle Surface Characteristics

Of the two nanoparticle suface characteristics used in this study, the first category was the manufacturer carboxylic acid surface treated f>CNT and f>GNP, which provided COOH functional groups on the surface of the nanoparticles. The carboxyl (C(=O)OH) group is an organic compound that has both carbonyl (C=O) and hydroxyl (OH) groups, which attach to carbon atoms. These groups usually attach to the carbon atoms of CNT and GNP at defect and end sites. They allow increased bonding and cross-linking between the nanoparticles and the VE matrix. As displayed in Figure 2, the as-received f>CNT showed very weak absorptions near 1705 cm^{-1}, which fall in the carboxyl acid range (1725 to 1700 cm^{-1}) of the carbonyl expansion [7]. These peaks indicated the presence of C=O bonds and confirmed that the carbon nanotubes were COOH functionalized. Furthermore, the slight peak around 1600 cm^{-1}, demonstrated the presence of conjugated ketone and amide (low C=O) bonding [7]. The f>GNP, on the other hand, did not exhibit any peaks that corresponded with COOH functionalization. Because of these results, we believe that both the f>CNT and f>GNP had negligible COOH funcationalization, when compared to nf>CNT and nf>GNP. Hence, system 1 (f>GNP-f>CNT/VE) produced the lowest K_{IC} and G_{IC} increases over neat-VE.

The second type of nanoparticle surface characteristics used in this investigation was TX100 surface treated f>CNT, f>GNP, nf>CNT and nf>GNP. Referencing Figure 2, f>CNT-TX100 and f>GNP-TX100 demonstrated similar peaks to TX100 near the following wavenumbers: 2940 (C-H, CH_2 and CH_3); 2850 (C-H, CH_2 and CH_3); 1610 (C=C), 1510 (C=C); 1450 (CH_3); 1390 (C-H and C-CH_3); 1345 (C-H and C-CH_3); 1245 (O-H); 1185 (C-O-C); 1100, 1065 and 1010 [8]. Additionally, the wavenumber regions of 1620-1400 and 1200-1000 indicated the presence of the TX100 benzene ring in the form of ring mode bonding and in-plane C-H bending, respectively [8]. As for the nf>CNT-TX100 nanoparticles, Figure 2 signaled very minor peaks at 2800, 1510, 1365, 1240, 1185 and 1100. These weak peaks established a presence of TX100 on the nf>CNT surface, albeit in less magnitude than with the previously described nanoparticles. The nf>GNP-TX100 did not show any evidence of TX100 surface treatment, and as such, the FTIR spectrum was not included in Figure 2. Figure 3 further shows the inability of TX100 to surface treat the nf>GNP. We posit that the nf>GNP did not have many defect sites, and thus, TX100 did not adequately attach to the surface.

When nf>CNT and nf>GNP were TX100 surface treated simultaneously, as in system 3, the solution showed substantial dispersion properties. Both nanoparticles remained suspended in solution after one week of being sealed and stored at room temperature. In system 3, we suspect that the nf>CNT was surface treated by TX100, and concurrently coupled to the surface of the nf>GNP in a perpendicular configuration.

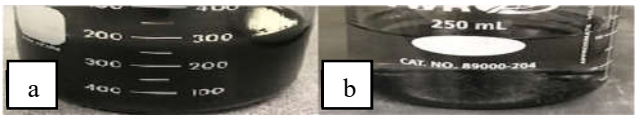

Figure 3: Comparing TX100 treated nanoparticles 24 hours after treatment (a) nf>CNT-TX100 (b) nf>GNP-TX100.

3.2 Nanoparticle Surface Characteristics

Since we previously completed an iterative process to find the optimized CNT and GNP concentrations, we knew

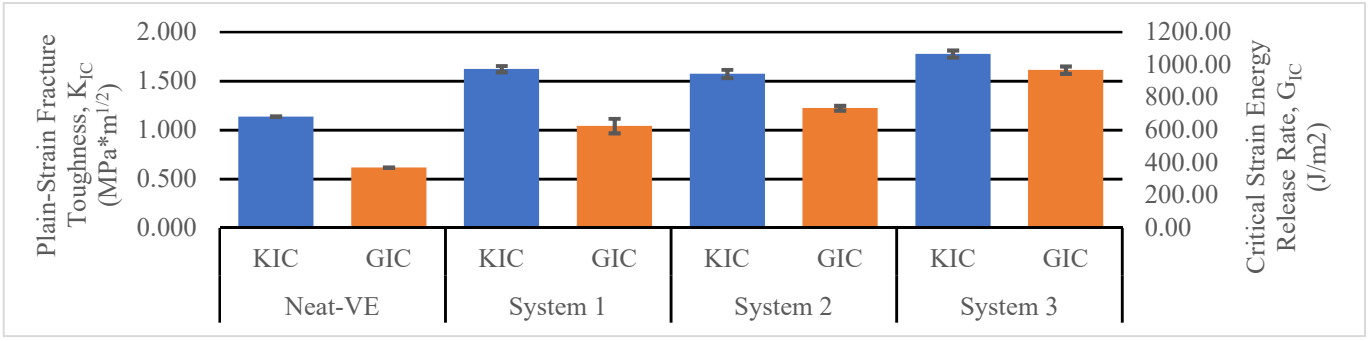

Figure 4: Average K_{IC} and G_{IC} for Neat-VE (1.137 and 370.3), System 1 (1.623 and 624.9), System 2 (1.573 and 734.1) and System 3 (1.777 and 967.5). Error bars represent one standard deviation.

that all three OHN systems would demonstrate substantial increases in K_{IC} and G_{IC} over the Neat-VE. Furthermore, we expected systems 2 and 3 to have the greatest fracture toughness increases because of their TX100 treatment. As Figure 4 shows, the average K_{IC} and G_{IC} increases over Neat-VE values were the following: 42.7% and 68.8% (system 1); 38.3% and 98.2% (system 2); 56.3% and 161.3% (system 3).

We postulate that three-dimensional nanostructures (3DN), where CNT absorbed perpendicular to the GNP surface, formed in the OHN, as described by Zhang and Liu [9]. We believe that the presence of the 3DN provided a two-fold synergistic enhancement of the K_{IC} and G_{IC}, as proposed by Yang et al. [10]. The CNT wedged in-between individual graphene nanoplatelets, which impeded GNP face-to-face aggregation and allowed the CNT to perpendicularly attach to the GNP surface. The resulting 3DN maintained the large surface area feature of GNP. This enlarged contact area allowed for greater cross-linking between 3DN and polymer chains. Additionally, the CNT functioned as extended tentacles. The tentacles intertwined with the VE polymer chains, again resulting in higher cross-linking density and better 3DN/VE interactions.

Upon further examination of Figure 4, systems 1 and 2 revealed a similar improvement in K_{IC} over neat-VE. The gains were even more evident with G_{IC}. Since both systems 1 and 2 were exactly the same except for the nanoparticle surface characteristics, we surmise that the TX100 treated f>CNT and f>GNP in system 2 were more able to evenly disperse into the VE matrix. Referencing Figure 2, the nanoparticles in system 2 had the highest degree of surface functionalization in this study. We believe these surface characteristics caused less nanoparticle agglomerations and increased nanoparticle dispersive power. We also posit that the surface characteristics yielded more cross-linking density between the VE and nanofillers, which led to greater G_{IC} values over both neat-VE and system 1.

In system 3, there were even more impressive K_{IC} and G_{IC} gains. Because the FTIR results in Figure 2 did not show much TX100 surface treatment with the nf>CNT and nf>GNP, we presume that the physical differences between the nf>nanoparticles and f>nanoparticles were the source of the highest fracture toughness values in system 3. The f>CNT employed in systems 1 and 2 had an aspect ratio of ~158, while the nf>CNT utilized in system 3 had an aspect ratio of ~2500. Perez et al. [11] demonstrated sharp fracture toughness improvements of CNT/epoxy composites, when using CNT with higher aspect ratios. We posit that the much higher aspect ratio of the nf>CNT played a major role in the fracture toughness increases. Furthermore, the nf>GNP and f>GNP had the same small diameter of 1-2µm. Chong et al. [12] and Wang et al. [13] discovered that smaller sized graphene platelets included in polymer increased the fracture toughness in the nanocomposite.

3.3 Nanocomposite Thermal Properties

Hybrid inclusions of CNT and GNP have been shown to enhance the T_g and T_p of the resulting nanocomposite. Hsieh et al. [14] uncovered a 5°C increase in the T_g for hybrid nanocomposites, when compared to neat-epoxy. Moosa et al. [15] revealed a 4 to 7°C growth in the devastation temperature (50% weight loss) for GNP-MWCNT/epoxy versus neat-epoxy composites. As Table 1 displays, all three OHN systems showed modest (4 to 7°C) improvements in the T_g and negligible (2 to 5°C) increases in the T_p. We attribute the improvements to the ability of GNP to efficiently dissipate heat.

System	Average T_g (°C)	Average T_p (°C)
Neat-VE	123.1	406.2
System 1	127.5	411.0
System 2	129.1	408.6
System 3	130.4	409.8

Table 1: Average T_g and T_p for all systems studied.

4 CONCLUSION

This paper showed that the fracture and mechanical traits of nanocomposites can be appreciably increased by adjusting the physical and surface charcateristics of the included nanoparticles. We believe that the highest K_{IC} and G_{IC} values seen in system 3 were a direct result of the high aspect ratio of the nf>CNT, small diameter of the nf>GNP and slight TX100 surface treatment of the 3DN. We attribute the minor T_g and negligible T_p increases in systems 1-3 to the large surface area of GNP. This allowed the GNP and 3DN to act as “heat sinks” and efficiently draw out heat from the OHN.

REFERENCES

[1] S. Iijima, Nature, 354, 56–58 (1991).
[2] N. Domun, H. Hadavinia, T. Zhang, T. Sainsbury, G.H. Liaghat and S. Vahid, Nanoscale 7 (23), 10294-10329 (2015).
[3] Y. Li, R. Umer, A. Isakovic, Y.A. Samad, L. Zheng and K. Liao, RSC Adv., 3, 8849-8856 (2013).
[4] R. Rastogi, R. Kaushal, S.K. Tripathi, A.L. Sharma, I. Kaur and L.M. Bharadwaj, J. Coll. Int. Sci., 328 (2), 421-428 (2008).
[5] ASTM D5045-14, West Conshohocken, PA (2014).
[6] ASTM E1356-14, West Conshohocken, PA (2014).
[7] J. Coates, Encycl. Anal. Chem., 10815–10837 (2000).
[8] B. Smith, Infrared Spectral Interpretation: A Systematic Approach (1998).
[9] C. Zhang and T.X. Liu, Chin. Sci. Bull. 57 (23), 3010-3021 (2012).
[10] S.-Y. Yang, W.-N. Lin, Y.-L. Huang, H.-W. Tien, J.-Y. Wang, C.-C.M. Ma, S.-M. Li and Y.-S. Wang, Carbon 49 (3), 793-803 (2011).
[11] H.A. Perez, F. Aviles, M.A. Pat, V.A. Gonzalez, H.P. Franco and B.P. Perez, Compos. Sci. Technol. 68 (6), 1422–1431 (2008).
[12] H.M. Chong, S.J. Hinder and A.C. Taylor, J. Mat. Sci. 51 (19), 8764-8790 (2016).
[13] X. Wang, J. Jin and M. Song, Carbon 65, 324-333 (2013).
[14] T.H. Hsieh, A.J. Kinloch, A.C. Taylor and S. Sprenger, Appl. Polym. Sci. 119 (4), 2135–2142 (2011).
[15] A.A. Moosa, A. Ramazani S.A., F.A.K. Kubba and M. Raad, Amer. J. Mat. Sci. 7 (1), 1-11 (2017).